THE ASTROPHYSICAL JOURNAL, 345:245–256, 1989 October 1

THE RELATIONSHIP BETWEEN INFRARED, OPTICAL, AND ULTRAVIOLET EXTINCTION

JASON A. CARDELLI, GEOFFREY C. CLAYTON, AND JOHN S. MATHIS
Wasburn Observatory, University of Wisconsin-Madison
Received 1989 January 12; accepted 1989 March 24

ABSTRACT

Using the parameterized extinction data of Fitzpatrick and Massa for the ultraviolet, and various sources for the optical and near-infrared, a meaningful average extinction law, $A(\lambda)/A(V)$, is derived over the wavelength range 3.5 μm $\geq \lambda \geq$ 0.125 μm, which is applicable to both diffuse and dense regions of the interstellar medium. The derived mean extinction law depends on only one parameter, which is chosen to be $R_V[=A(V)/E(B-V)]$. An analytic formula is given for the mean extinction law which can be used to calculate color excesses or to deredden observations. The formula closely reproduces the mean extinction laws of Seaton and Savage and Mathis for values of R_V near 3.1, the value in the diffuse interstellar medium. However, there are real deviations of individual lines of sight from the mean law at all values of R_V. These deviations are especially large for $\lambda < 0.16$ μm.

The mean R_V-dependent extinction law presented here is tentatively extended beyond the range of the *IUE* satellite to 0.10 μm on the basis of the four stars observed in this wavelength range by the *Copernicus* satellite, plus the extension of the analytic fits to the *IUE* spectra by Fitzpatrick and Massa. In addition, $E(0.10\ \mu\text{m}–0.13\ \mu\text{m})/A(V)$ for 12 stars for which the color data are available is in excellent agreement with $E(0.10–0.13)/A(V)$ derived from the extension of the Fitzpatrick and Massa analytic fits.

We confirm the result of others that the shape of the extinction law for long wavelengths ($\lambda > 0.7$ μm) is independent of R_V to within the errors of measurements. Because of systematic variations at the V filter, the choice of normalizing the extinction law to $A(V)$ introduces a spurious dependence of the longer wavelengths on R_V and normalization to some wavelength longward of V (e.g., >0.7 μm) would be more logical. However, normalization at V was chosen because of the wealth of data there.

From the analytic results presented here, the poor correlation of $[A(0.13\ \mu\text{m})–A(0.17\ \mu\text{m})]$ with $E(B-V)$, and the much better correlation of $[A(0.22\ \mu\text{m})–A(0.25\ \mu\text{m})]$ with $E(B-V)$ can be understood through the specific R_V-dependencies exhibited by these colors.

The existence of the mean extinction law, valid over a large wavelength interval, suggests that the processes which modify the sizes and compositions of grains are stochastic in nature and very efficient. Apparently all sizes are modified simultaneously. When changes in the small grains responsible for the far-ultraviolet extinction occur, the entire size distribution apparently varies in a systematic way.

The accretion of the small amounts of refractory elements (Al, Mg, Fe, etc.) which are observed to be more depleted in dense regions than in the diffuse cannot add much to grain volumes. For two well-observed dark cloud stars (ρ Oph and NU Ori), the extinction per H nucleus, integrated over the observed wavelengths, is smaller than in the diffuse interstellar medium. For many other stars the situation is not so clear, because of the difficulty of estimating the column density of hydrogen, but is likely to be similar. These observations imply that grains are larger in the clouds because of their sticking together (coagulating) rather than accreting extensive mantles.

The parameter R_V seems well related to the strength of the λ2175 bump but not to the central wavelength or the width of the bump. The dependence of the "far-UV rise," $\lambda < 0.16$ μm, on R_V is not discussed because the mathematical representation is probably more formal than physical.

Subject headings: interstellar: matter — ultraviolet: spectra

I. INTRODUCTION

Interstellar extinction can show a large range of variability from one line of sight to another. While the wavelength dependence of this variability is well documented in the UV (0.32 μm $> \lambda >$ 0.09 μm; for a recent review of the observations, see Massa and Savage 1989), there can also be significant variability in at least part of the optical (0.7 μm $> \lambda >$ 0.32 μm). The extent of the variability of the infrared extinction law (for $\lambda > 0.7$ μm) is not yet clear. However, from existing broadband data, variability *in the shape* of IR extinction seems relatively minor (Jones and Hyland 1980; Clayton and Mathis 1988; Whittet 1989; see also the discussion in § III*a* below).

The shapes of extinction curves can be conveniently compared if $A(\lambda)$, the absolute extinction at any wavelength, is expressed relative to $A(\lambda_{\text{ref}})$, the absolute extinction at a chosen reference wavelength. Probably the most logical choice of λ_{ref} is a wavelength for which variability in the shape of the extinction at longer wavelengths is small or nonexistent (e.g., $\lambda_{\text{ref}} >$ 0.7 μm). However, since so many observations exist for the yellow portion of the spectrum, the visual extinction, $A(V)$, is used as the reference for historical reasons.

Extinction has often been analyzed using a two-color normalization of the form $E(\lambda-V)/E(B-V)$. However, the true nature of the variability of observed extinction may be hidden by the choice of normalization. The quantity $A(\lambda)/A(V)$ is in some sense a more fundamental extinction law than $E(\lambda-V)/E(B-V)$ because the absolute extinction is expressed directly, rather than by comparing one color with another. There are

some relationships which emerge more clearly when $A(\lambda)/A(V)$ is considered than when normalization by $E(B-V)$ is used. In this paper, we will use the expression "extinction law" to mean $A(\lambda)/A(V)$, unless otherwise noted.

Recently, very careful UV extinction studies of 45 stars (Fitzpatrick and Massa 1986, FM86; Fitzpatrick and Massa 1988, FM88) have encouraged the study of the relationship between the optical and UV portions of the extinction law, primarily because the UV extinction was accurately determined and conveniently parameterized by simple analytic expressions. By combining these UV results with optical and near-IR (NIR) photometry, Cardelli, Clayton, and Mathis (1988, CCM) showed that there is a strong relationship between the shape of absolute optical and UV extinction laws for lines of sight considered by FM86 and FM88. They parameterized the extinction laws by using $R_V[\equiv A(V)/E(B-V)]$, derived from the optical/NIR extinction, which can also serve as an indicator of certain environmental characteristics. The algebraic expression given in CCM for the mean R_V-dependent UV extinction law shows large systematic differences in extinction for lines of sight with considerably different values of R_V. For instance, for $R_V = 3.1$, the standard value for the diffuse interstellar medium (ISM), the mean value of $E(0.125\ \mu\text{m} - V)/E(B-V)$ is 6.55 (Savage and Mathis 1979). If $R_V = 5$, a value found in some dense clouds, the mean extinction law given in CCM yields $E(0.125\ \mu\text{m} - V)/E(B-V) = 3.56$. Clearly, significant errors will result if one applies the diffuse ISM extinction law to the situation in which $R_V = 5$. Cardelli (1988) has emphasized the importance of the differences in R_V-dependent UV extinction curves for the abundances of interstellar molecules, which are often observed in regions where R_V is larger than the value typical for the diffuse ISM (see also Cardelli and Brugel 1988; Cardelli and Wallerstein 1989).

FM86 and FM88 analyzed the values of $E(\lambda-V)/E(B-V)$ in the UV in terms of a superposition of three mathematical expressions, at least one of which probably has physical meaning as well. These expressions are (FM88): (*a*) a term linear in $x(\equiv 1/\lambda\ \mu\text{m}^{-1})$, $(c_1 + c_2 x)$; (*b*) a "Drude profile," which is an expression representing the 2175 Å "bump"; and (*c*) the "far-UV rise," the part of the UV extinction law which increases rapidly with x for values of $x > 5.9\ \mu\text{m}^{-1}$ (see also Greenberg and Chlewicki 1983; GC). The "Drude profile" (Bohren and Huffman 1983) is the absorption coefficient of a "free" electron with some dissipation. The Drude profile has three parameters: c_3, proportional to the strength of the bump; γ, related to the FWHM of the bump; and λ_0, the central wavelength of the bump. The far-UV rise term is a specific cubic polynomial with a coefficient c_4 which is determined by the fitting procedure. The $E(\lambda-V)/E(B-V)$ in the UV for each line of sight is described extremely well by the six parameters c_1–c_4, γ, and λ_0 (FM88). With such an analytic representation, observations are easy to reproduce and analyze which makes quantitative comparisons among the various stars in the FM sample possible.

At any given value of R_V, most observed extinctions deviate from CCM's mean R_V-dependent extinction law by more than the observational errors. Such mean deviations, shown in CCM and in Figure 4 for several wavelengths, are especially large at small wavelengths ($x > 7\ \mu\text{m}^{-1}$). These deviations limit the accuracy with which one can correct the energy distributions of reddened objects using the CCM analytic expression. However, one should bear in mind that the standard galactic extinction laws (e.g., Seaton 1979; Savage and Mathis 1979) represent the mean extinction law for *one particular value of* R_V, about 3.1. Even lines of sight with $R_V \approx 3.1$ deviate as much from these standard extinction laws as from the CCM expression, and the deviations become increasingly large and systematic as R_V deviates from 3.1. For $R_V > 3.5$, the systematic deviations are larger than the dispersion about the mean for the lines of sight at the same R_V. Thus, while the accuracy of the CCM expression has limits, it represents *a mean interstellar law at every* R_V.

In this paper, we will (*a*) provide more observational foundation for the correlations of the optical and the UV extinction laws than was possible in CCM; (*b*) by means of a polynomial in x, extend the analytic expression of CCM into the optical/NIR and the wavelength range 0.12 μm–0.10 μm (this latter range is based on limited data); and (*c*) discuss some of the relationships between the various UV parameters defined in FM88 and the optical parameter R_V. We will also discuss the implications of these relationships upon the physical nature of interstellar dust.

II. OBSERVATIONAL DATA AND THE DETERMINATION OF ABSOLUTE EXTINCTIONS

We considered all lines of sight in FM88 for which near-infrared (NIR) photometry (defined here as measurements of the stellar colors in at least one of the Johnson [1966] filters K or L, plus at least one of the filters J or H) could be found. Most lines of sight had observations at all nine filters of the series U, B, V, R, I, J, H, K, and L. For consistency, the intrinsic colors of Johnson (1966) for the appropriate spectral types (from FM88) were used to determine the extinctions. The source of data are given in Clayton and Mathis (1988) and Clayton and Cardelli (1988). With these extinctions we then (*a*) determine the visual extinction, $A(V)$; (*b*) from $A(V)$ and $E(\lambda-V)$, $A(\lambda)$ and $R_V = A(V)/E(B-V)$ follow; (*c*) for the whole sample of stars (hereafter, the FM sample) we compare one variable of interest (e.g., the bump, the far-UV rise component, etc.) to another (generally R_V^{-1}, for which the relationship appears to be linear in nature).

We have utilized two methods of computing $A(V)$, both of which use an adopted standard curve. The first assumes that all extinction laws for $\lambda > 0.55\ \mu$m (the V filter) have the form given by Rieke and Lebofsky (1985, RL), which has $R_V = 3.08$. Let us denote $A(\lambda)/A(V)$ for the RL extinction law by $f_{\text{RL}}(\lambda)$. The visual extinction for the kth star, $A_k(V)$, is determined by minimizing the quantity $\chi^2 = \Sigma_i[E_k(\lambda_i - V) - A_k(V) f_{\text{RL}}(\lambda_i)]^2$. Here, i represents all the filters R, I, J, H, K, and L for which the data exist, and the λ_i are the effective wavelengths for the filters. From $A_k(V)$ and the observed colors, $E_k(\lambda-V)$, all other extinctions are known, and $A_k(\lambda)/A_k(V)$ follows. This method has the advantage of being objective and quantitative, but it is subject to errors if some of the extinction data are "clearly" not correct, which can occur when the NIR is contaminated by emission (Cardelli and Clayton 1988). Furthermore, there are systematic R_V-dependent differences among the extinction laws of various lines of sight which begin to become noticeable near V for $R_V > 4$ but are generally not sufficient to significantly affect the derived value of the visual extinction until $R_V > 5$.

The second method of determining $A_k(V)$ involves an interactive graphical comparison, over the wavelength range J, H, K, and L, between the RL curve and the observed kth curve, plotted against $x[\equiv 1/\lambda(\mu\text{m}^{-1})]$. The two curves are plots of $Cf_{\text{RL}}(\lambda)$ and $A_k(V) + E_k(\lambda-V)$, where C and $A_k(V)$ are con-

stants. The best fit is found by adjusting C and $A_k(V)$ until the two curves match over the interval $\lambda \geq 1.25$ μm. We assume that the shapes of extinction curves over this range are independent of R_V. This method assumes that the actual extinction law is like that of RL *only for* $\lambda \geq \lambda(J) = 1.25$ μm and simply uses $f_{RL}(\lambda)$ as a guide to extrapolate the extinction curve out to infinite wavelength, where the extinction must go to zero.

For our sample, the R_V values calculated from the two methods agree to better than 5% with the exception of six stars for which $R_V > 4.5$. For these objects, deviation from the standard curve is quite apparent at V. In addition, for three of these objects (θ^1 Ori C, θ^1 Ori D, and Herschel 36), there is obvious contamination by infrared emission longward of the H passband ($\lambda = 1.65$ μm). For these stars, the results of method 2 are adopted (in the case of contamination by IR emission, fitted to the R, I, and J data only). The adopted data appear in Table 1.

III. EMPIRICAL RELATIONSHIPS

a) *Relations of $A(\lambda)/A(V)$ and R_V*

CCM discussed plots of $A(\lambda)/A(V)$ against R_V^{-1} for the FM sample of stars for the wavelength range of 0.32 $\mu m > \lambda > 0.12$ μm. The resulting plots are close to linear, and CCM gave an analytic expression for the linear relationship $A(\lambda)/A(V) = a(x) + b(x)/R_V$. There is also a similar linear relation between $A(\lambda)/A(V)$ and R_V^{-1} for extinction in the visual/NIR spectral region. The analytic formula for $a(x)$ and $b(x)$, which is repeated here (with minor modification) and extend as equations (2)–(4) below, is a good representation of the best linear fit to the relation between $A(\lambda)/A(V)$ and R_V^{-1} for 3.4 $\mu m \geq \lambda \geq 0.12$ μm.

TABLE 1

OBSERVATIONAL DATA

HD (E) or BD	Name	Spectral Type	$E(B-V)$	R_V[a]
14250	Oo 1586	B1 III	0.57	2.85
34078	AE Aur	O9.5 V	0.53	3.42
36982	LP Ori	B2 V	0.34	5.60
37022	θ^1 Ori C	O6 p	0.34	5.50
37023	θ^1 Ori D	B0.5 V	0.37	5.23
37061	NU Ori	B0.5 Vp	0.54	5.10
37903	...	B1.5 V	0.35	4.11
38087	...	B3 n	0.33	5.30
46202	...	O9 V	0.47	3.12
48099	...	O7 V	0.27	3.52
73882	...	O8.5 V((n))	0.72	3.39
93028	...	O9 V	0.24	3.92
93222	...	O7 III((f))	0.40	4.98
147701	...	B5 V	0.73	4.04
147888	ρ Oph D	B3 V:	0.52	4.13
147889	...	B2 V	1.09	4.20
147933/4	ρ Oph AB	B2 IV + V	0.47	4.34
149757	ζ Oph	O9.5 V	0.32	3.09
154445	...	B1 V	0.42	3.15
164740	Herschel 36	O7.5 V(n)	0.89	5.30
167771	...	O7 III:(n)((f))	0.44	3.48
193322	...	O9 V:((n))	0.41	3.05
204827	...	B0 V	1.11	2.60
229196	...	O6 II(n)(f)	1.22	3.12
252325	...	B0 IV	0.87	3.33
+56°524	Oo 1078	B1 Vn	0.60	2.75
−59°2600	...	O6 V((f))	0.53	4.17
	Oo 936	B1.5 V	0.55	2.84
	Tr 14 No. 20	O6 V	0.60	3.71
NGC 2244 average	...	...	...	3.33
Cep OB III average	...	...	...	3.3
LMC average	...	...	...	3.1

[a] $R_V \equiv A_V/E(B-V)$.

TABLE 2

COEFFICIENTS AND STANDARD DEVIATIONS AT SELECTED WAVELENGTHS

λ (μm)	x (μm^{-1})	$a(x)$[a]	$b(x)$[a]	σ[b]
0.125	8.00	−1.0705	13.670	0.320
0.15	6.67	−0.4086	9.5342	0.190
0.18	5.56	−0.09472	8.1091	0.150
0.2175	4.60	0.00032	9.8896	0.195
0.25	4.00	0.3581	6.0738	0.117
0.3125	3.20	0.7004	3.2792	0.065
0.36	2.78	0.9530	1.9090	0.022
0.44	2.27	0.9982	1.0495	...
0.55	1.82	1.0000	0.0000	...
0.70	1.43	0.8686	−0.3660	0.017
0.90	1.11	0.6800	−0.6239	0.027
1.25	0.80	0.4008	−0.3679	0.030
1.6	0.63	0.2693	−0.2473	0.034
2.2	0.46	0.1615	−0.1483	0.040
3.4	0.29	0.0800	−0.0734	0.060

[a] Derived from eqs. (2), (3), and (4).

[b] Standard deviation of the observed data about the best fit of $A(\lambda)/A(V)$.

Figure 1*a* shows plots of $A(\lambda)/A(V)$ and R_V^{-1} for $\lambda = 0.12$ μm, 0.22 μm (also shown in CCM), 0.28 μm, and 0.70 μm (the R filter). One can see that at each wavelength, there is a good linear relationship between $A(\lambda)/A(V)$ and R_V^{-1}. From our derivation of $A(V)$, we find that the mean error in R_V is approximately $0.05R_V$. This uncertainty is shown in Figure 1*a* (and all subsequent figures with R_V^{-1} as the abscissa) for two values of R_V^{-1}. Figure 1*b* is the same as Figure 1*a* except for $\lambda = 0.15$ μm, 0.22 μm, and 0.33 μm. The FM sample from which the analytic expression was produced is shown as filled symbols. Also shown (*open symbols*) are lines of sight from many directions in the Galaxy, taken from the *ANS* extinction excess catalog of Savage *et al.* (1985) for which optical/NIR data were available. No extinction/spectral class criteria were used in data selection. The requirements for inclusion into the catalog are discussed in Savage *et al.* (1985) and include the omission of objects with spectral types later than B8. A number of the stars are supergiants, for which the intrinsic colors are less well known than for the stars in the FM sample. Furthermore, the spectral types of the ANS stars could not be determined directly from the UV data, as they could from the *IUE* data used by FM86 and FM88. Nevertheless, the *ANS* data closely fit the same relationship as the FM sample. We take this to indicate that the FM sample is an unbiased representation of the average R_V-dependent behavior, even though it contains lines of sight that have traditionally been viewed as having "peculiar" UV extinction.

As seen in Figures 1*a* and *b*, there are real deviations from the mean relationship at each wavelength. The mean deviation seems to be independent of R_V, so we can average over all R_V to estimate the standard deviation. Table 2 gives the standard deviations of the observed points from the best-fit values of $a(x) + b(x)/R_V$ at selected wavelengths. These deviations set a practical limit to the accuracy with which observations can be corrected for extinction, even if the value of R_V is known precisely. Note that the deviations are much larger at 0.12 μm than at other wavelengths. Also note that inclusion of the *ANS* data in Figure 1*b* does not appreciably change the deviation of the $a(x) + b(x)/R_V$ fit or the dispersion, in spite of the presumably lower quality of the derived extinction excesses.

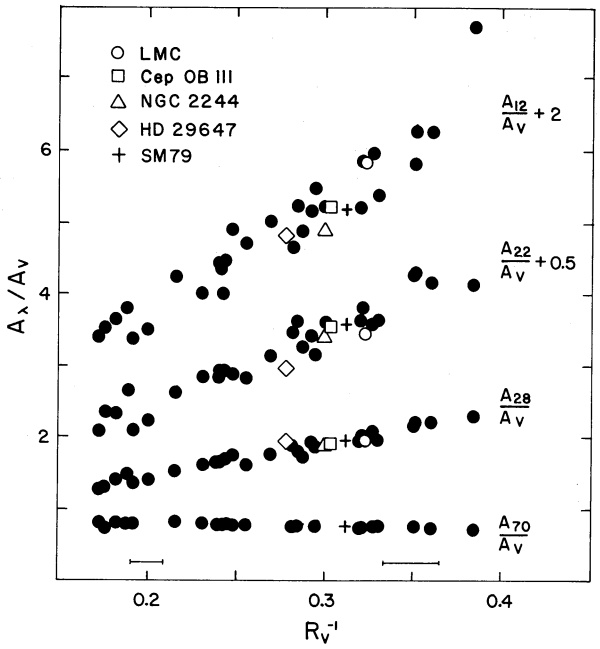

FIG. 1a

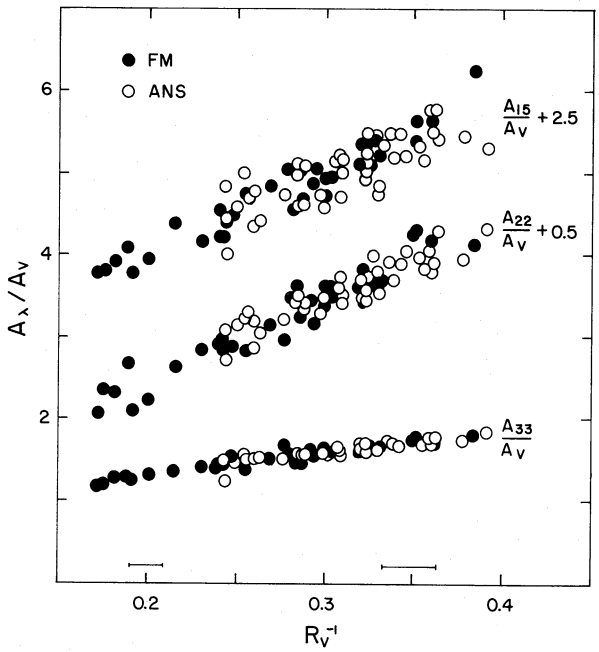

FIG. 1b

FIG. 1.—(*a*) The extinction ratio $A(\lambda)/A(V)$ plotted against $R_V^{-1}[\equiv E(B-V)/A(V)]$ at selected wavelengths for data from the FM sample (see Table 1). The subscripts refer to the wavelength [e.g., $A_{12} \equiv A(0.12\ \mu m)$, etc.]. The data for 0.12 μm and 0.22 μm have been shifted vertically by the amount indicated in order to separate them. The "error" bars represent the mean uncertainty in R_V at two values (see text). Also shown (*open symbols*) are the average data for the LMC and two clusters from the FM sample. The data for HD 29647 are derived from the extinction fit of Cardelli and Savage (1988). The plus symbol represents $A(\lambda)/A(V)$ for the average curve ($R_V = 3.1$) of Savage and Mathis (1979: SM79). With the exception of 0.12 μm, the SM79 curve appears to correspond to the mean $A(\lambda)/A(V)$ vs. R_V^{-1} relation. (*b*) Same as (*a*) except for the wavelengths 0.15 μm, 0.22 μm, and 0.33 μm. The filled symbols represent the data from the FM sample. The open symbols represent data obtained from the *ANS* extinction excess catalog of Savage *et al.* (1985) for which we had optical/NIR data. Again, the data for 0.15 μm and 0.22 μm have been shifted vertically in order to separate them.

Figure 1*a* shows that extinction laws, expressed as $A(\lambda)/A(V)$, certainly vary with R_V at wavelengths shorter than V. The question is: at long wavelengths, is this variation the result of using $A(V)$ to normalize the extinction? In other words, is there some wavelength, λ_0, such that extinction laws for all lines of sight, $A(\lambda)/A(\lambda_0)$, are the same function within the observational errors for $\lambda \geq \lambda_0$? The shortest such wavelength would be the best choice of normalizing the various extinction laws, since the extinction law for all longer wavelengths would then be independent of direction. [Normalization with $A(V)$ is done for practical reasons—all the stars in the FM sample have observations at V and B, while some observations are missing for all other filters. There is also a strong historical precedent for expressing extinctions relative to $A(V)$; astronomers are used to expressing extinction laws in this way.]

Figure 2 illustrates the importance of the choice of normalization by showing $A(\lambda)/A(I)$ plotted against R_V^{-1} for filter effective wavelengths $\lambda = 0.44\ \mu m$ (B), 0.55 μm (V), 0.70 μm (R), and 1.25 μm (J). The effective wavelength of the I filter is 0.90 μm. The scatter is much greater than in Figure 1*a* because the extinction at I is smaller than at V, and the measurement errors are larger. Note that, like the plots of $A(\lambda)/A(V)$, the dependency for wavelengths shorter than the normalization wavelength exhibits a positive slope. However, notice that at $\lambda = 1.25\ \mu m$, the slope of the relationship is approximately zero. Although the data show a larger dispersion, the same result is found for $\lambda > 1.25\ \mu m$ (H, K, and L filters). Within the observational errors, *the data are consistent with a single extinction law for at least* $\lambda \geq 0.90\ \mu m$ (Jones and Hyland 1980; Koornneef 1983; RL; Smith 1987; Whittet 1989). The wavelength at which all extinction laws become similar may be

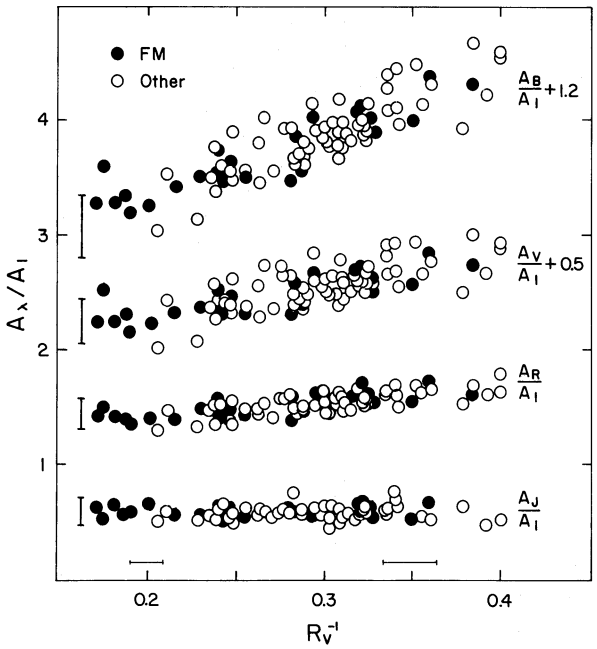

FIG. 2.—The extinction ratio $A(\lambda)/A(I)$ plotted against R_V^{-1} at selected optical/NIR wavelengths where $\lambda(I) = 0.90\ \mu m$. The subscripts B, V, R, and J refer to the wavelengths of the Johnson filters (see Table 3). The filled symbols represent data for the FM sample. The open symbols represent data for other lines of sight for which we had optical/NIR data. The vertical "error" bars represent the mean uncertainty of the extinction ratios derived from the propagation-of-errors of the uncertainty in $A(V)$ and the various observed colors (e.g., $B-V$, $V-I$, etc., see text). Again, the data for B and V have been shifted vertically in order to separate them. In comparison to Fig. 1*a*, the data presented here indicate that normalization by $A(I)$ is probably a better choice, since the dependence on R_V appears minor for $\lambda \geq I$.

between 0.90 μm and 0.70 μm, but we are unable to determine this due to the limited wavelength sampling of the data. The long-wavelength extinction law determined by Elias, Frogel, and Humphreys (1985), which is based on data for stars with a variety of values of R_V, is completely consistent with the RL law. There are minor differences between the various near-IR extinction laws when presented in terms of color-excess ratios [e.g., $E(J-H)/E(H-K)$], but we have not investigated their origins. The increased scatter in $A(\lambda)/A(I)$ is another reason for presenting the results in terms of $A(\lambda)/A(V)$, even though the normalization to $A(V)$ produces a spurious dependence on R_V which is not really presented at wavelengths longer than about 0.9 μm.

The filled symbols in Figure 2 represent data for a subset of the FM sample for which data at R, I, and J were available. The open symbols represent a large sample of additional data for which we had optical/NIR photometry. Most of these data come from the list given in Clayton and Cardelli (1988). As with Figure 1*b*, these data, which number 70 lines of sight, clearly show that the behavior exhibited by the FM sample is a good representation of the average R_V-dependence. The "error" bars shown in the figure represent mean uncertainties calculated via a propagation-of-errors analysis using the adopted mean observational color errors discussed in CCM and calculated uncertainties in the derived $A(V)$ values. Although the scatter within the relationships shown in Figure 2 may represent real systematic deviations from the mean, the scatter is within the limits of the observational uncertainties.

b) Parameterization: The Average R_V-dependent Extinction Law

Using NIR and optical data for stars in FM sample, we have extended the fitting of $\langle A(\lambda)/A(V)\rangle$, the mean extinction law, to the range 0.3 μm^{-1}–3.3 μm^{-1}, while CCM considered only 3.2 $\mu m^{-1} < x < 8$ μm^{-1}. The procedure was the same as the one used by CCM and involved deriving the least-squares coefficients a_i and b_i from a linear fit to $A(\lambda_i)/A(V)$ versus R_V^{-1} at all the optical passband wavelengths (see Table 3). The wavelength-dependent coefficients $a(x)$ and $b(x)$ were then fitted with a polynomial in x, in units of μm^{-1}. The mean R_V-dependent extinction law then takes the form

$$\langle A(\lambda)/A(V)\rangle = a(x) + b(x)/R_V \ . \quad (1)$$

For computational reasons, the complete extinction curve (0.3 μm^{-1}–8 μm^{-1}) has been divided into three wavelengths regions: *infrared* ($\lambda \geq 0.9$ μm), *optical/NIR* (0.9 $\mu m \geq \lambda \geq 0.3$ μm), and *ultraviolet* (0.3 $\mu m \geq \lambda \geq 0.125$ μm). In addition, a *far-ultraviolet* (0.125 $\mu m \geq \lambda \geq 0.10$ μm) segment has been added. The far-UV segment is based on only limited data (York *et al.* 1973; Snow and York 1975; Jenkins, Savage, and Spitzer 1986) and is therefore more uncertain. The division of the complete curve into segments is also practical in that it roughly defines different instrument/observing regimes. The results are discussed below.

TABLE 3

COEFFICIENTS AND EXTINCTION AT STANDARD OPTICAL/NEAR-IR WAVELENGTHS

				$A(\lambda)/A(V)$ for $R_V = 3.1$		
FILTER	$x(\mu m^{-1})$	$a(x)$[a]	$b(x)$[a]	$a(x)+b(x)/R_V$	SM79[b]	RL[c]
U	2.78	0.9530	1.9090	1.569	...	1.531
B	2.27	0.9982	1.0495	1.337	1.322	1.325
V	1.82	1.0000	0.0000	1.000	1.000	1.000
R	1.43	0.8686	−0.3660	0.751	0.748	0.748
I	1.11	0.6800	−0.6239	0.479	0.484	0.482
J	0.80	0.4008	−0.3679	0.282	0.281	0.282
H	0.63	0.2693	−0.2473	0.190	...	0.175
K	0.46	0.1615	−0.1483	0.114	0.123	0.112
L	0.29	0.0800	−0.0734	0.056	0.052	0.058

[a] Derived from eqs. (2) and (3).
[b] From Savage and Mathis (1979) for their adopted R_V of 3.1.
[c] From Rieke and Lebofsky (1985) for their adopted R_V value of 3.1.

i) *The Infrared and Optical*

Infrared: 0.3 $\mu m^{-1} \leq x \leq 1.1$ μm^{-1};

$$a(x) = 0.574x^{1.61} \ ; \quad (2a)$$

$$b(x) = -0.527x^{1.61} \ . \quad (2b)$$

Optical/NIR: 1.1 $\mu m^{-1} \leq x \leq 3.3$ μm^{-1} and $y = (x - 1.82)$;

$$a(x) = 1 + 0.17699y - 0.50447y^2 - 0.02427y^3 + 0.72085y^4 + 0.01979y^5 - 0.77530y^6 + 0.32999y^7 \ ; \quad (3a)$$

$$b(x) = 1.41338y + 2.28305y^2 + 1.07233y^3 - 5.38434y^4 - 0.62251y^5 + 5.30260y^6 - 2.09002y^7 \ . \quad (3b)$$

Figure 3 shows a comparison of the computed optical/NIR portion of the curve from equations (2) and (3) with data for three lines of sight with widely separated values of R_V. The positions of the different passbands are also labeled. The fit is quite good for all three lines of sight. Because $A(\lambda)/A(I)$ seems independent of R_V for $\lambda \geq 0.9$ μm, the segment for $x \leq 1.1$ μm^{-1} was derived by fitting the data of RL with a power law.

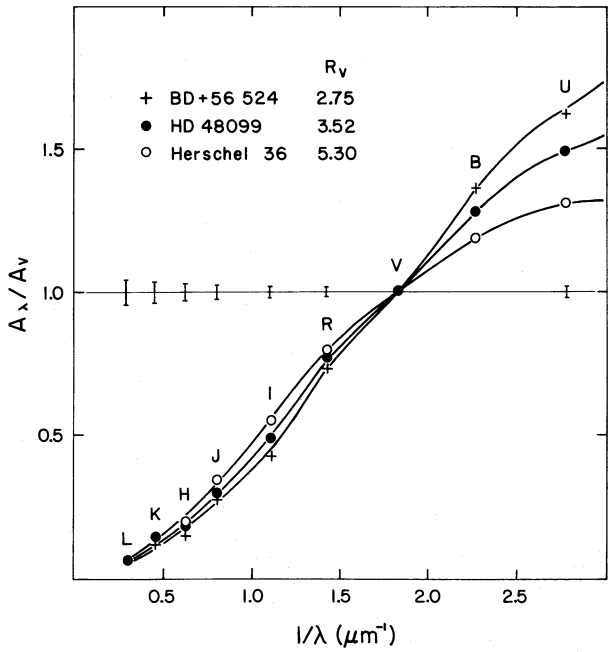

FIG. 3.—Comparison between the mean optical/NIR R_V-dependent extinction law from eqs. (2) and (3) and three lines of sight with largely separated R_V values. The wavelength position of the various broad-band filters from which the data were obtained are labeled (see Table 3). The "error" bars represent the computed standard deviation of the data about the best fit of $A(\lambda)/A(V)$ vs. R_V^{-1} with $a(x) + b(x)/R_V$ where $x \equiv \lambda^{-1}$. The effect of varying R_V on the shape of the extinction curves is quite apparent, particularly at the shorter wavelengths.

The equation for the segment 1.1 $\mu m^{-1} \leq x \leq 3.3$ μm^{-1} was found by fitting a seventh-order polynomial to $a(x)$ and $b(x)$ derived from $A(\lambda)/A(V)$ versus R_V^{-1} at the passbands I through U and the UV point at $x = 3.3$ μm^{-1}. The "error" bars shown in the figure are the standard deviations of the data at each passband about the best fit. Very likely, they do not represent true errors, but rather the real deviations of various lines of sight from the mean. Although we only have data at the wavelengths indicated, a polynomial was used in order to allow the mean extinction to be directly calculated at all wavelengths. (A preliminary optical/NIR extinction law was given in Cardelli, Clayton, and Mathis 1989. While that law reproduces the average R_V-dependent extinction reasonably well, we consider the results of eqs. [3a] and [3b] as a more accurate representation.)

How do our R_V-dependent results compare to standard average curves? Table 3 lists the values of $a(x)$, $b(x)$, and $A(\lambda)/A(V)$ for $R_V = 3.1$ from equations (2) and (3) at the various wavelengths where data were available, along with $A(\lambda)/A(V)$ for the same R_V from the average curves of Savage and Mathis (1979; SM79) and RL. The agreement is quite good at all wavelengths. Comparison between $A(\lambda)/A(V)$ from equations (2) and (3) and a spline or interpolation of the SM and RL data for other wavelengths indicates no significant deviation between B and L (this is only a comparison to using SM or RL, and does not include the presence of *real* structure). However, our polynomial shows a slight enhancement in extinction, or hump, between B and U amounting to $+0.05$ at $x = 2.50$ μm^{-1}. This hump is not present in the data of SM79 and is probably due to our fit. Consequently, the *R_V-dependent* results of equations (2) and (3) can be equally reproduced (without the hump) from a spline fit or interpolation of the values of $a(x)$ and $b(x)$ supplied in Table 2.

How does our function compare to higher resolution curves? The well-known Whitford (1958) extinction law, recently confirmed by Ardeberg and Virdefors (1982), has two segments, linear in x, joining at $x = 2.25$ μm^{-1} (see also Underhill and Walker 1966). Because the optical portion of our polynomial extinction law was derived from broad-band data, equation (2) does not have the abrupt change in slope (perhaps the hump produced from our polynomial fit is a consequence of this rapid change in slope). The Whitford law may therefore be more accurate for the diffuse ISM near $x \approx 2.25$ μm^{-1}. The virtue of ours, however, is that it joins smoothly onto the UV extinction law from the FM sample of stars, and that it takes into account the *differences in the extinction laws of lines of sight with various values of R_V*. Our extinction law also does not contain any of the very broad band structure which has been reported in the optical extinction law (Hayes *et al.* 1973; Schild 1977; Walker *et al.* 1980; Krelowski, Maszkowski, and Strobel 1986). We have not analyzed the data upon which the Whitford law was based to see if there are any effects introduced by combining lines of sight with different values of R_V into the same mean law.

ii) *The Ultraviolet and Far-UV*

Ultraviolet: 3.3 $\mu m^{-1} \leq x \leq 8$ μm^{-1};

$$a(x) = 1.752 - 0.316x - 0.104/[(x - 4.67)^2 + 0.341] + F_a(x) \quad (4a)$$

$$b(x) = -3.090 + 1.825x + 1.206/[(x - 4.62)^2 + 0.263] + F_b(x) \quad (4b)$$

$$F_a(x) = -0.04473(x - 5.9)^2 - 0.009779(x - 5.9)^3 \quad (8 \geq x \geq 5.9)$$

$$F_b(x) = 0.2130(x - 5.9)^2 + 0.1207(x - 5.9)^3 \quad (8 \geq x \geq 5.9)$$

$$F_a(x) = F_b(x) = 0 \quad (x < 5.9)$$

Figure 4 shows a comparison between our R_V-dependent extinction law from 0.3 $\mu m^{-1} \leq x \leq 8$ μm^{-1} for the same three lines of sight shown in Figure 3. Because the curves are closely spaced in the optical/NIR, only the optical data at U, B, and V have been shown. The agreement is quite good, especially for Her 36 and BD +56°524. HD 48099 has been shown, because it represents one of the poorer fits in the sample. Again, the "error" bars shown in the figure are the standard deviations of the data (e.g., Fig. 1*a*) about the best fit. (Eq. [4] is identical with the one found in CCM with the exception of the first term in eq. [4a], which has been decreased by 0.05. This decrease represents only a zero-point shift in the UV curve presented by CCM and was found to be necessary in order to smoothly join the optical with the UV. Such a small shift is well within the dispersion of the data.)

As with the optical/NIR, one test of the consistency of the above UV expressions is to compare reddening corrections produced using equation (4) with existing average curves, the most quoted of which are SM79 and Seaton (1979; S79). In the case of equation (4), the appropriate R_V value is adopted to be 3.1–3.2. Differences between normalized reddening corrections, $A(\lambda)/A(V)$, produced from equation (4) and those from the

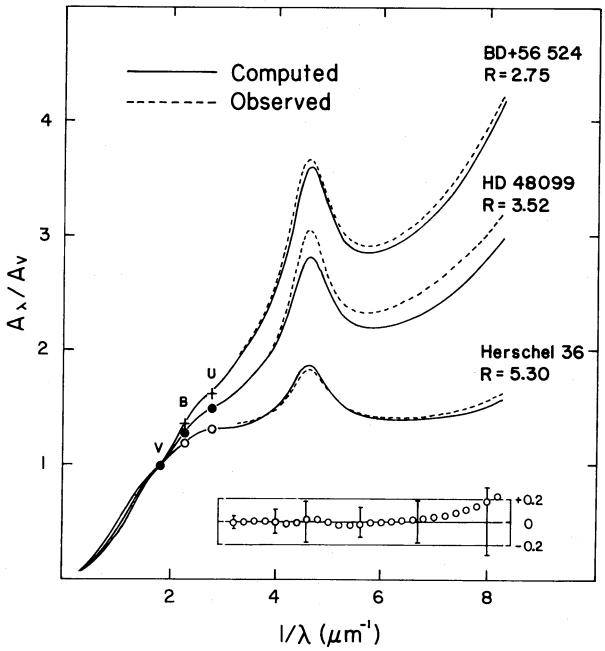

FIG. 4.—Same as Fig. 3 except for the UV portion of the mean R_V-dependent extinction law from eq. (4). The data at U, B, and V from Fig. 3 are also plotted. Again, the "error" bars in the lower inset represent the computed standard deviation of the data about the best fit of $A(\lambda)/A(V)$ vs. R_V^{-1} with $a(x) + b(x)/R_V$. The open symbols in the inset represent the difference between $A(\lambda)/A(V)$ from eq. (4) and the average curve of Seaton (1979) for $R_V = 3.2$. The only serious deviation occurs for $x > 7$ μm^{-1} (see text).

average curve of S79 are shown in the lower inset in Figure 4. The SM79 curve was derived from the same data as S79 and is very similar, except that it is given only in tabular form. For $x < 7\ \mu m^{-1}$, the differences are less than $\pm 4\%$. However, for $x > 6.7\ \mu m^{-1}$, the deviation between $A(\lambda)/A(V)$ from equation (4) and S79 becomes increasingly larger. While we do not necessarily assume that the behavior of equation (4) for $x > 6.7\ \mu m^{-1}$ is more correct for $R_V \approx 3.2$, the possibility exists that the differences from the average curves are related to the way in which these average curves were derived. The SM79 and S79 curves were derived by averaging extinction curves for which individual values of R_V were not known, but were *presumably* not significantly different than 3.2. In addition, the applicable UV portion of these average curves was created by splicing two different extinction data sets together at $x \approx 7\ \mu m^{-1}$. Equation (4), on the other hand, was determined by considering extinction at all R_V values (e.g., $6 > R_V > 2.5$) for a single data set representing the entire UV range from $3.2\ \mu m^{-1} \leq x \leq 8.3\ \mu m^{-1}$.

For $x \approx 8.3\ \mu m^{-1}$, the value of $A(0.12\ \mu m)/A(V)$ for SM79 and S79 is shown in Figure 1*a*. As can be seen, this value is inconsistent with the mean relationship and it would seem unreasonable to alter the fit to accommodate this point. Because of the good agreement between our mean extinction law and SM79 and S79 for $x \leq 7\ \mu m^{-1}$, we doubt that our data suddenly exhibit systematic errors at this wavelength. Unlike the FM88 data, for which spectral types were derived from the UV spectra, the extinction data used by SM79 and S79 probably include larger mismatches in both temperature and luminosity class, the effects of which are most pronounced at short wavelengths (SM79 note the presence of luminosity mismatch in their curve). Also, since serious discrepancies first appear at the point where a different extinction data set is used in the SM79 and S79 average curves, the possibility exists that an R_V value different from the one appropriate for $x < 7\ \mu m^{-1}$ part of the curve applies. From a comparison to equation (4), the slope of the average curve segment between $7\ \mu m^{-1} \leq x \leq 9\ \mu m^{-1}$ is consistent with $R_V \approx 3.4$–3.5. We therefore conclude that *our curve more accurately represents the average extinction between* $7 \mu m^{-1}$ *and* $8\ \mu m^{-1}$.

Far-UV: $8\ \mu m^{-1} \leq x \leq 10\ \mu m^{-1}$;

$$a(x) = -1.073 - 0.628(x - 8) + 0.137(x - 8)^2 - 0.070(x - 8)^3 ; \quad (5a)$$

$$b(x) = 13.670 + 4.257(x - 8) - 0.420(x - 8)^2 + 0.374(x - 8)^3 . \quad (5b)$$

Equation (5) has been included for completeness and was derived by extrapolating the FM88 cubic far-UV function beyond $8\ \mu m^{-1}$ to $10\ \mu m^{-1}$. Because there is little complete data over this wavelength region (only one star in our sample, ζ Oph, has complete data in this range), this portion of the curve is more uncertain. Figure 5 shows a comparison of $A(\lambda)/A(V)$ for $6\ \mu m^{-1} \leq x \leq 10\ \mu m^{-1}$ from equations (4) and (5) with data for the stars ζ Oph, ζ Per, ξ Per (York *et al.* 1973), and σ Sco (Snow and York 1975). Also shown is the standard deviation about the best fit to the data from the FM sample at several wavelengths. Each pair of curves (computed and observed) has been shifted by an amount C for clarity. Note that, with the exception of σ Sco, the general shapes of the observed curves are well represented by the average R_V-dependent law down to $x = 10\ \mu m^{-1}$; the agreement is

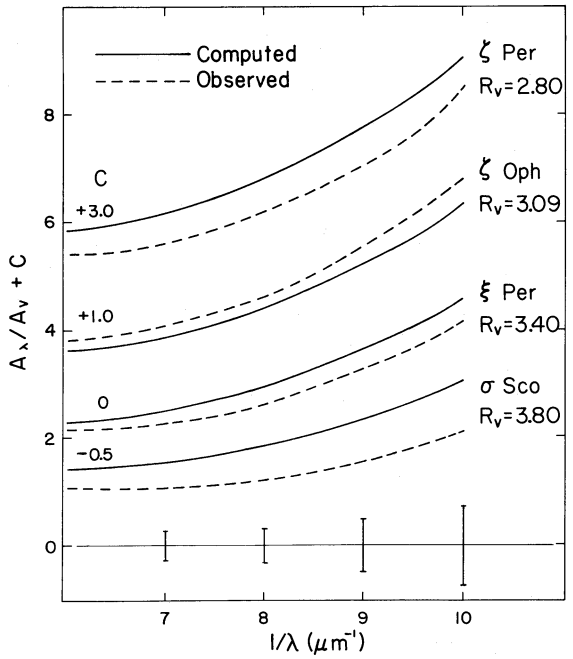

FIG. 5.—Comparison between the far-UV portion of the mean R_V-dependent extinction law from eq. (5) and four lines of sight for which data for $x > 8\ \mu m^{-1}$ were available. The computed and observed curve for each star have been shifted vertically by an amount C in order to separate them. Again, the "error" bars represent the computed standard deviation of the data about the best fit of $A(\lambda)/A(V)$ vs. R_V^{-1} with $a(x) + b(x)/R_V$. Although our mean extinction law was derived by fitting data corresponding to an extrapolation of the FM88 far-UV function beyond $x = 8\ \mu m^{-1}$, the *shape* of the observed curvature is fitted quite well for three of the stars.

about as good at the wavelengths where the fit was extrapolated ($x > 8\ \mu m^{-1}$) as it is at wavelengths where there are real data ($x \leq 8\ \mu m^{-1}$). The quality of the far-UV function is also supported by Figure 6, which shows the difference in extinction between $\lambda = 0.1054\ \mu m$ and $0.1347\ \mu m$ [the color $E(1054-1347)$] normalized to $A(V)$ plotted against R_V^{-1}. The filled symbols represent the FM sample and the open symbols are from the *Copernicus* data of Jenkins, Savage, and Spitzer (1986; Table 1A-extinction E_6). The data for the four lines of sight in Figure 5 are labeled. The distribution of the normalized *Copernicus* color data are consistent with the normalized color derived from an extrapolation of the FM88 far-UV function; most of the *Copernicus* points lie within the 1 σ deviations of the FM data. Thus, from Figures 5 and 6, we conclude that (1) extrapolation of the FM88 cubic far-UV function beyond $x \approx 8\ \mu m^{-1}$ is a fair representation of the actual extinction on average, and (2) equation (5) is a fair representation of the average R_V-dependent extinction law for $x > 8\ \mu m^{-1}$. We note that the SM79 curve for $x \geq 9\ \mu m^{-1}$ consists of the average of data of only three lines of sight, two of which are shown in Figures 5 and 6 (ζ Per and ξ Per).

c) Relationship among the UV and Optical Extinction Parameters

FM88 characterized the UV extinction for each of the stars in their sample by a superposition of three simple analytic functions involving six free parameters. The extinction is written in the form

$$FM(x) \equiv E(\lambda - V)/E(B-V) = c_1 + c_2 x + c_3 D(\gamma, x_0) + c_4 P(x) , \quad (6)$$

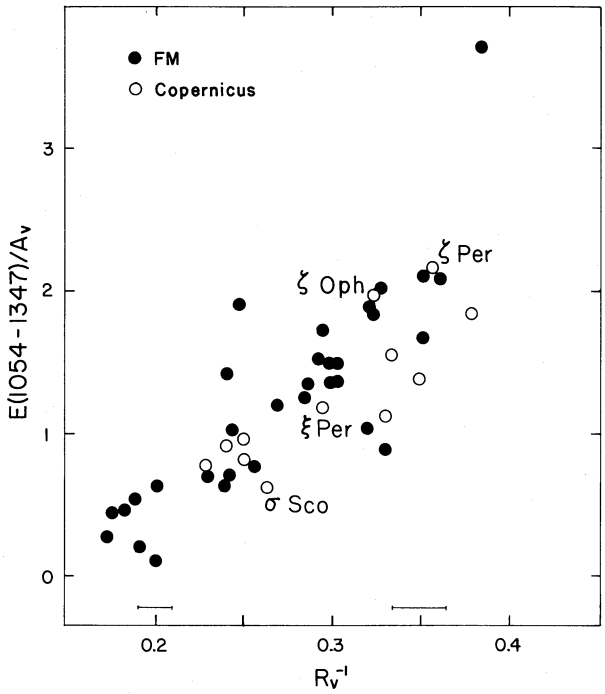

FIG. 6.—The difference in extinction between 0.1054 μm and 0.1347 μm [the color $E(1054\text{–}1347) \equiv A(1054)\text{–}A(1347)$] normalized to $A(V)$ plotted against R_V^{-1}. The filled symbols represent data from the FM sample. The data at $A(1054)$ were derived from an extrapolation of the FM88 far-UV function. The open symbols represent *Copernicus* data taken from Table 1A (extinction E_6) of Jenkins, Savage, and Spitzer (1986). Most of the *Copernicus* color data are within the 1 σ dispersion of the FM data. On average, the slope of the far-UV extinction is fairly well represented by an extrapolation of the FM88 far-UV function.

where $D(\gamma, \lambda_0)$ is the Drude function, γ is the bump FWHM, $x_0 (\equiv \lambda_0^{-1})$ is the central wavenumber of the bump, and $P(x)$ is a cubic polynomial for $x > 5.9$ μm^{-1} and zero otherwise. Since we are considering extinction in the form $A(\lambda)/A(V)$, we have instead

$$A(\lambda)/A(V) = [FM(x)E(B-V)/A(V)] + 1 = [FM(x)/R_V] + 1 . \quad (7)$$

While the decomposition of an extinction law into analytic expressions might be misleading if there is no physical basis for the forms chosen (other than that they adequately represent the observed extinction law), there is a physical basis for assuming that the bump can be represented by a Drude function. The Drude function is in the form of absorption profile of a freely oscillating electron subject to damping.

FM86 discussed many of the properties of the bump, and showed that there are no convincing correlations among the bump parameters. The strongest correlation is that bumps along lines of sight in dense material appear to be broader than those in the more diffuse ISM. We now discuss how the UV extinction parameters are correlated with R_V.

We define A_{bump}, the "bump strength," to be the excess extinction of the bump over the linear part of the fit to the extinction law. From FM88, we have $A_{bump}/A(V) = c_3/(\gamma^2 R_V)$. Figure 7 is a plot of $A_{bump}/A(V)$ against R_V^{-1}. The filled symbols represent the FM sample. The open symbols represent the same *ANS* data set shown in Figure 1*b*. These data were converted to A_{bump} using the relation $E(2200-V) - E(1500-V)/2 - 0.62E(B-V)$. This relation was empirically derived from lines of sight in the FM data set for which *ANS* data were also available. The comparison of $A_{bump}/E(B-V)$ from c_3/γ^2 with $A_{bump}/E(B-V)$ calculated from the *ANS* data using the above empirical relation is shown in Figure 8.

Usually, extinctions are plotted in the form $E(\lambda-V)/E(B-V)$. Figure 9 shows this quantity for the bump, again plotted against R_V^{-1}. Again, the filled symbols represent the FM sample while the open symbols are from the *ANS* sample. Since $R_V = A(V)/E(B-V)$, we have $A_{bump}/E(B-V) = [A_{bump}/A(V)]R_V \equiv c_3/\gamma^2$. Figure 9 contains exactly the same information as Figure 7, but the points at each R_V^{-1} have been spread out by a factor of R_V. The relationship between the bump strength and R_V is less obvious than when $A_{bump}/A(V)$ is considered (Fig. 7).

Figure 7 shows that the *mean* bump strength is a linear function of R_V. There is, of course, real dispersion about the mean relation. From the dependence seen in Figure 7, it might be tempting to imagine that the grains responsible for the bump are related to those responsible for the variations in the optical extinction and R_V. If this were true, then one might expect that γ and x_0 also show systematic variations with R_V. Figures 10*a*, *b* show a comparison between γ and x_0, and R_V^{-1}. Both figures clearly show scatter diagrams, indicating that the parameters intrinsic to the bump are independent of R_V. The dependence of $A_{bump}/A(V)$ on R_V^{-1} is secondary, in that both probably result from the way in which the grains are processed to yield different R_V values.

IV. DISCUSSION

The most important result presented here is that the entire mean extinction law, from the near-IR through the optical and

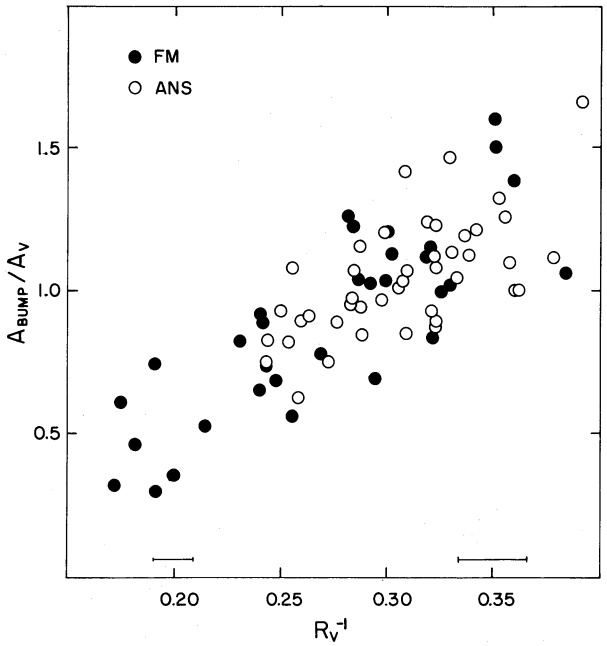

FIG. 7.—The absolute bump strength, A_{bump}, normalized to $A(V)$ plotted against R_V^{-1}. The filled symbols represent the data from the FM sample [$A_{bump} \equiv (C_3/\gamma^2)E(B-V)$; see text]. The open symbols represent data from the same *ANS* sample of stars as in Fig. 1*b*. For the *ANS* data, A_{bump} was computed from an empirical expression derived from the FM88 data for which *ANS* data also exist (see Fig. 8). The data clearly show that the mean bump strength per unit $A(V)$ is dependent on R_V^{-1}.

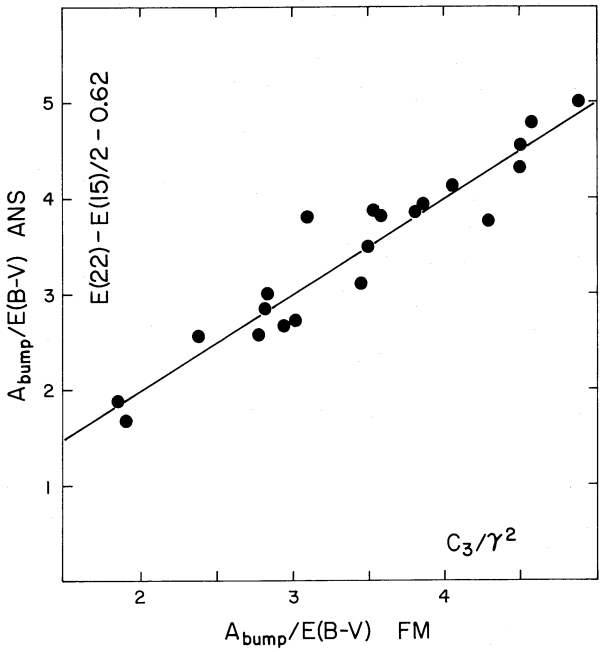

FIG. 8.—The empirical relationship between $A_{bump}/E(B-V)$ derived from the data of FM88 and the *ANS* data of Savage *et al.* (1985) for a sample of stars common to both data sets. The solid line is not a formal fit, but simply corresponds to a slope of unity and a zero intercept. The empirical relationship from which $A_{bump}/E(B-V)$ was calculated from the *ANS* data appears along the vertical axis $[E(22) \equiv E(22-V)/E(B-V)$ and $E(15) \equiv E(15-V)/E(B-V)]$.

IUE-accessible UV, can be well represented by a mean relationship which depends upon a single parameter. We have chosen to use R_V for convenience, but it has no particular physical significance. No doubt other well-observed quantities similarly defined could have served in its stead.

The significance of the one-parameter nature of the mean extinction law is that it shows that the processes which produce changes in extinction operate effectively and rather continuously over most or all of the range of grain sizes and compositions; the deviations of the observations from the mean relation (e.g., Figs. 1 and 2) are impressively small. Even though there are rather different physical conditions in the ISM even along the various lines of sight to stars which have the same values of R_V, the extinction law is characterized quite well by R_V alone. One can easily imagine that this would not be the case. If diverse types of grains provide most of the extinction at various wavelengths, we would expect that some processes would modify a particular component (e.g., the far-UV rise) and leave others unchanged. However, in the real ISM the processes which modify the extinction at one wavelength also seem to modify the entire mean extinction law in a regular way. The processes for modifying grains must be general and stochastic in nature, so that grains of all but the largest sizes participate to an appreciable extent. Since it is not clear whether the extinction law at the longest wavelengths

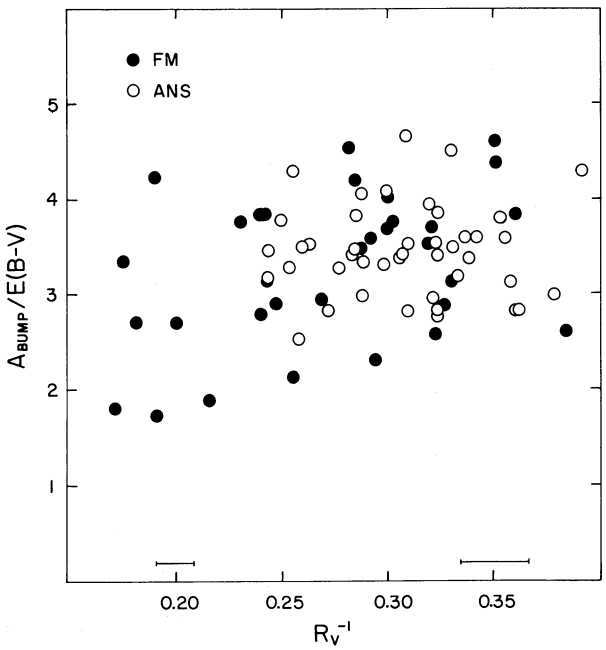

FIG. 9

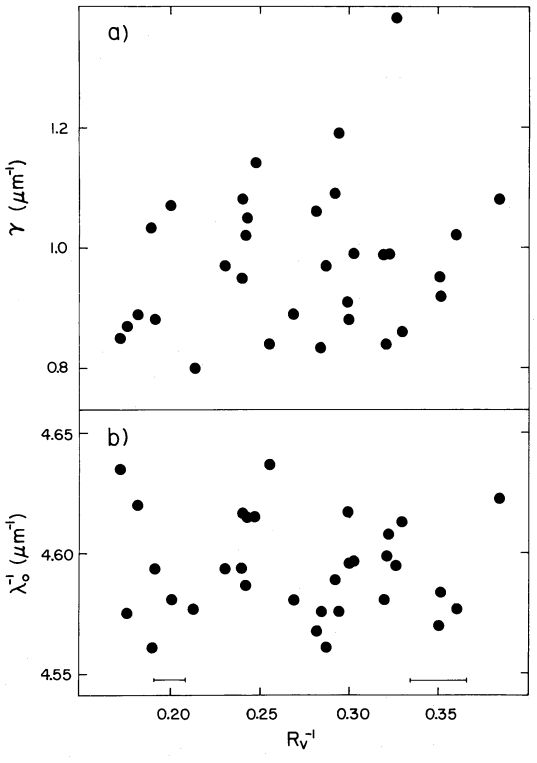

FIG. 10

FIG. 9.—The absolute bump strength, A_{bump}, normalized to $E(B-V)$ plotted against R_V^{-1}. The source of the data is the same as in Fig. 7. Although the data shown here contain the same information as in Fig. 7, $A_{bump}/E(B-V)$ shows no dependence on R_V. This figure clearly points out how the interpretation of extinction can depend upon the choice of normalization, particularly $E(B-V)$.

FIG. 10.—The (*a*) bump FWHM (γ) and (*b*) central wavenumber (λ_0^{-1}) plotted against R_V^{-1} for the FM sample. Unlike the $A(V)$ normalized bump strength (Fig. 7), the width and central position of the bump are uncorrelated with R_V^{-1}. This indicates that the bump carrier is independent of the grains responsible for variations in R_V. The mean dependence of $A_{bump}/A(V)$ on R_V^{-1} could be interpreted as a systematic variation of the *available number of bump grains with* R_V via their incorporation into coagulated aggregates for which "bump extinction" is suppressed.

varies among the various lines of sight, we reserve judgment as to the modifications of the largest grains.

At first glance our results seem at variance with those of GC, who investigated the extinction for $x > 6\ \mu m^{-1}$, called the "far-UV rise." GC found that $A(0.13\ \mu m)$–$A(0.17\ \mu m)$ [$\equiv E(13–17)$] is poorly correlated with $E(B-V)$. In contrast, they found that the bump strength, expressed as $A(0.22\ \mu m)$–$A(0.25\ \mu m)$ [$\equiv E(22–25)$], is almost proportional to $E(B-V)$, with a correlation coefficient of 0.946 for their sample of stars. GC also found that the curvature in the extinction law for $x > 6\ \mu m^{-1}$ is constant for the stars in their sample. They concluded that the far-UV rise must be contributed by small particles (whose extinctions per unit mass are independent of the size distribution because they are in the "Rayleigh limit"), and that the size distributions of the large particles which contribute to the visual extinction along various lines of sight vary independently from those which produce the far-UV rise. In the light of the GC data, both of these conclusions are reasonable. However, in the discussion in the preceding paragraph, we concluded that whatever processes modify the size distribution in one regime act in a rather systematic fashion over the entire size distribution.

How can these views be compatible? The answer seems to be that one of the ratios GC considered, $E(13–17)/E(B-V)$, is very sensitive to R_V, while the other, $E(22-25)/E(B-V)$, is not. By means of equations (2)–(4) the dependence of any color index on R_V can be determined by simply subtracting the expressions for the relevant extinctions. We find by direct calculation from the mean extinction laws that

$$E(13–17)/E(B-V) = 4.16 - 0.73R_V; \quad (8a)$$

$$E(22–25)/E(B-V) = 3.81 - 0.36R_V . \quad (8b)$$

Equations (8) show that for the differences of the values of R_V found in various regions, 2.7 to at least 5, there is considerable difference, a factor of 4, in the right-hand side of equation (8a). The right-hand side of equation (8b) varies far less (a factor of 1.4) because of much less cancellation of the two terms. The slope of the $E(22–25)$–$E(B-V)$ relation in GC is about 2.6, consistent with that predicted from equation (8b) for $R_V \approx 3.4$. This explanation of the differences in the scatter in the two ratios is consistent with HD 147889 ($R_V = 4.20$) being especially discrepant in GC's $E(22–25)$–$E(B-V)$ diagram.

There are also real variations from our mean extinction law, and these variations will introduce scatter into the color index ratios given in equations (8). The dispersion is especially large at 0.13 μm, so the actual scatter should be appreciably worse than equation (8a) would suggest. Formal "errors" are not given for the coefficients in equations (8) because the deviations in the various colors are, no doubt, far from random. Deviations on the extinction at 0.13 μm appear to be highly correlated with deviations at 0.17 μm (Cardelli and Mathis 1989).

Our results call into question the reasoning of GC that if the shape of extinction laws are the same in various directions, the particles producing that extinction must be small. The shapes of the extinction laws are related over the entire wavelength range we have investigated. The similarities in shapes must be produced by similarities of the processes which modify grain size distributions, rather than by having the wavelength dependence of the extinction independent of the distribution.

a) Why Are Grains Larger in Dense Regions?

There are many processes which can modify the grain size or composition distribution (see Seab 1987 for a review). Collisions between grains can lead to both shattering and sticking together, or coagulation. In cold dense regions, grains can accrete mantles of materials from the gas phase, which we will call "accretion." Deep within molecular clouds, icy mantles form in this way, perhaps starting with water and ammonia ices and continuing to frozen CO. Shocks can lead to sputtering of large grains and violent grain-grain collisions upon passage through the shock, or to evaporation of small grains because of their immersion in very hot shock-heated gas.

The differences in the extinction laws between small and large values of R_V are almost surely caused by there being systematically larger particles in dense regions, although Chini and Krügel (1983) produced some counterexamples to this notion. They confined their calculations to the optical/NIR portions of the spectrum, and we suspect that the addition of the UV strengthens the conclusion that the mean grain size increases with R_V. Direct calculations attempting to fit large-R_V extinction laws over the UV and optical regions of the spectrum (Mathis and Wallenhorst 1981; Duley, Williams, and Jones 1989; Mathis and Whiffen 1989; MW) have all needed a size distribution skewed toward substantially larger particles.

We cannot believe that the larger mean grain size in dense regions is achieved through the sputtering or evaporation of the small grains, because the refractory elements (Fe, Mg, Ca, etc.) appear to be more depleted in dense regions than in the diffuse ISM (Jenkins, Savage, and Spitzer 1986; Joseph 1988). The greater depletion in dense regions shows that there must be some grain growth by accretion, but the refractory elements alone can only increase the total volume of grains by 5%. Appreciable growth by accretion must involve elements with large abundances (C, N, and O).

A directly observable difference between accretion and coagulation is that accretion increases the volume of the grain, and therefore the total extinction cross section per H nucleus. Coagulation can either increase or decrease this quantity, depending upon the details of the initial and final size distributions. For a given mass of grains, the total extinction, integrated over wavenumber, can be reduced by clumping the matter into large grains in which the inner material is shielded from the radiation by the outside. On the other hand, modest growth of grains can increase the extinction per gram by allowing the constituent atoms to absorb collectively.

Let us consider the integrated extinction law, $A_{int}(R_V)$, which is easy to calculate using the extinction laws given in equations (2)–(4). If we adopt equation (5) as representative of the extinction beyond $x = 8\ \mu m^{-1}$, we can integrate to $x = 10\ \mu m^{-1}$. The result of the integrations are

$$A_{int}(R_V) \equiv \int A(x)/A(V)(dx/x_V)$$

$$= 0.84 + 23.55\ R_V^{-1} \quad (0.8 \le x \le 8\ \mu m^{-1}) \quad (9a)$$

$$= -2.36 + 43.45\ R_V^{-1} \quad (0.8 \le x \le 10\ \mu m^{-1}) . \quad (9b)$$

Equations (9) show that the integrated extinction, relative to $A(V)$, is almost proportional to R_V^{-1}, and so is much smaller in dense regions (large R_V) than for the diffuse ISM.

The true integrated extinction, including the unobserved far-UV, is larger than either expression in equations (9), but the trend of $A_{int}(R_V)$ decreasing with R_V is almost certainly correct. The slope of $A(\lambda)/A(V)$ at the largest observed values of x is much smaller for large R_V than for small (see Fig. 4). We find it difficult to believe that some unknown source of far-UV extinc-

tion, which has no signature in the observed UV, overcomes the observed decrease of extinction with R_V.

To discuss coagulation versus accretion, the visual extinction per H nucleus, $A(V)/N(\mathrm{H})$, must be considered. In the diffuse ISM, $A(V)/N(\mathrm{H})$ is 5.3×10^{-22} mag cm^2 (Bohlin, Savage, and Drake 1978). For dense regions, observational data are rather uncertain because of the difficulty of determining $N(\mathrm{H})$, and in general there is a great deal of scatter in the relation between $A(V)/N(\mathrm{H})$ and R_V. The neutral H column density, $N(\mathrm{H\ I})$, is determined from the Lyman-α equivalent width (Shull and van Steenberg 1985; de Boer *et al.* 1986), and $N(\mathrm{H}_2)$ from the Lyman and Werner bands as observed with the *Copernicus* satellite (Savage *et al.* 1977). For the well-determined case of ρ Oph AB ($R_V = 4.4$), $A(V)/N(\mathrm{H\ I} + 2\mathrm{H}_2)$ is 0.8 times the value for the diffuse ISM (de Boer *et al.* 1986). For NU Ori ($R_V = 5.1$), $A(V)/N(\mathrm{H\ I}) = 0.73$ of the standard value (Shull and van Steenberg 1985), and correcting for $N(\mathrm{H}_2)$ will make the value decrease. Both $A(V)/N(\mathrm{H})$ and the integrated extinction per $A(V)$, equation (9), are smaller for these stars than for the diffuse ISM. For ρ Oph, $A_{\mathrm{int}}(R_V)/N(\mathrm{H})$ is 0.52 of the diffuse ISM value, and for NU Ori it is less than or equal to 0.43. These integrated extinction cross sections clearly show that increases in grain sizes must be strongly dominated by coagulation rather than accretion, at least for these two lines of sight. This result is consistent with, but stronger than, the consideration of $A(V)/N(\mathrm{H})$ alone (Jura 1980; Mathis and Wallenhorst 1981). The situation for the rest of the stars as regards $A(V)/N(\mathrm{H})$ is not so clear, but the decrease of the integrated extinction with R_V makes it likely that coagulation is the general rule.

b) *The λ2175 Å Bump*

The problems of identifying the carrier of the bump have been discussed elsewhere (FM86; Cardelli and Savage 1988; MW; Draine 1989). There is as yet no very credible identification, although the bump must arise from an abundant element. In this paper, we have found that there is a fairly good relationship (Fig. 7) between $A_{\mathrm{bump}}/A(V)$ and R_V^{-1} which is rather obfuscated by using $A_{\mathrm{bump}}/E(B-V)$ (Fig. 9). In contrast, Figure 10*a*, *b* indicates that the bump width, γ, and central wavelength, λ_0, exhibit no obvious relationship with R_V^{-1}.

Whatever the bump carrier is, it is less effective per $A(V)$ (and also per H nucleus) at large R_V than it is for small. The extinction law, $A(\lambda)/A(V)$, can be integrated from equation (4) for the bump alone, which yields

$$\int A_{\mathrm{bump}}(x)/A(V)\,dx = -0.56 + 7.39R_V^{-1}\ (\mu\mathrm{m}^{-1})\,. \quad (10)$$

The second term above is larger than the first, so that to a good approximation the mean bump strength is inversely proportional to R_V. If the carrier is a small particle (graphite?), as is strongly suggested by λ_0 being almost constant, then the mass fraction of the particles must decrease with R_V, since the extinction per mass is a constant for small particles. The particles which are free in the diffuse ISM must be incorporated into the larger grains which do not give rise to the bump. The independence of λ_0 from R_V makes it highly unlikely that coatings of some sort in dense regions can reduce the effectiveness of the bump carrier(s) enough to produce the relationship (10), since coatings, in general, shift λ_0 to longer wavelengths, as well as decrease the strength of the bump (Gilra 1972). The two most discrepant stars (Cardelli and Savage 1988) as regards λ_0 are at shorter wavelengths than the average.

One possibility is that polycyclic aromatic hydrocarbons (PAHs) produce the bump. Cox and Leene (1987) have argued against this hypothesis by determining the extinction ratio $A_{\mathrm{bump}}/E(B-V)$ of early-type stars lying behind cirrus, and comparing it with the *IRAS* 12/100 μm intensity ratio at that location. They found no relationship between the two quantities. Since the 12 μm *IRAS* filter is dominated by the infrared emission bands commonly attributed to PAHs, this observation suggests that PAHs are not responsible for the bump. However, we have already shown that using $E(B-V)$ to normalize extinction can lead to confusion if there are lines of sight with greatly different values of R_V involved in the sample, and the conclusion of Cox and Leene (1987) needs to be tested further using a normalization of $A(V)$.

Whatever produces the bump, the most likely explanation of the general decrease of the bump strength with R_V^{-1} without a systematic shift in λ_0 and width, is that the carrier of the bump is incorporated entirely into other grains. Small particles producing the bump likely stick to larger grains during the coagulation process. If they do, the resonance which produces the bump in the small, isolated particle is completely removed by the polarization charges produced by the passing electromagnetic wave on the rest of the large grain. The incorporation of bump carriers into other grains produces composite grains of some sort and is a motivation for the MW theory.

c) *The Far-UV Rise*

Figure 4 shows that the sum of the linear and far-UV rise extinctions decreases dramatically with R_V. The dependence of the far-UV extinction with R_V suggests that, in dense regions, the carrier of the far-UV rise, like the carrier of the bump, is also incorporated into the larger grains. However, we have not attempted to discuss the far-UV rise (e.g., c_4) in the same manner as the bump. The Kramers-Krönig relations ensure that, at some value of x, the assumed linear increase of extinction must break down. Consequently, the mathematical separation of the far-UV extinction law into a linear part and a cubic polynomial is merely formal mathematics, with little physical significance, while the fitting of the bump with a Drude profile does have real meaning.

We would like to thank B. D. Savage for his useful comments and suggestions during the course of this project and an anonymous referee for constructive comments on the text. We would also like to acknowledge partial support from contract K 957996 from the Space Astronomy Data Analysis Program (SADAP) from the Jet Propulsion Lab and NASA grants NAG5-832 and NAG5-1078.

REFERENCES

Ardeberg, A., and Virdefors, B. 1982, *Astr. Ap.*, **115**, 347.
Bohlin, R. C., Savage, B. D., and Drake, J. F. 1978, *Ap. J.*, **224**, 132.
Bohren, C. F., and Huffman, D. R. 1983, *Absorption and Scattering of Light by Small Particles* (NY: Wiley).
Cardelli, J. A. 1988, *Ap. J.*, **335**, 177.
Cardelli, J. A., and Brugel, E. W. 1988, *A.J.*, **96**, 673.
Cardelli, J. A., and Clayton, G. C. 1988, *A.J.*, **95**, 516.
Cardelli, J. A., Clayton, G. C., and Mathis, J. S. 1988, *Ap. J. (Letters)*, **329**, L33 (CCM).
———. 1989, in *IAU Symposium 135, Interstellar Dust*, ed. L. J. Allamandola and A. G. G. M. Tielens (Dordrecht: Reidel), in press.
Cardelli, J. A., and Mathis, J. S. 1989, in preparation.

Cardelli, J. A., and Savage, B. D. 1988, *Ap. J.*, **325**, 864.
Cardelli, J. A., and Wallerstein, G. 1989, *A.J.*, **97**, 1099.
Chini, R., and Krügel, E. 1983, *Astr. Ap.*, **117**, 289.
Clayton, G. C., and Cardelli, J. A. 1988, *A.J.*, **96**, 695.
Clayton, G. C., and Mathis, J. S. 1988, *Ap. J.*, **327**, 911.
Cox, P., and Leene, A. 1987, *Astr. Ap.*, **174**, 203.
de Boer, Lenhart, H., van der Hucht, K. A., Kramperman, T. M., Kondo, Y., and Bruhweiler, F. C. 1986, *Astr. Ap.*, **157**, 119.
Draine, B. T. 1989, in *IAU Symposium 135, Interstellar Dust*, ed. L. J. Allamandola and A. G. G. M. Tielens (Dordrecht: Reidel), in press.
Duley, W. W., Williams, D. A., and Jones, A. P. 1989, *M.N.R.A.S.*, **236**, 709.
Elias, J. H., Frogel, J. A., and Humphreys, R. M. 1985, *Ap. J. Suppl.*, **57**, 91.
Fitzpatrick, E. L., and Massa, D. 1986, *Ap. J.*, **307**, 286 (FM86).
———. 1988, *Ap. J.*, **328**, 734 (FM88).
Gilra, D. P. 1972, in *The Scientific Results of the Orbiting Astronomical Observatory OAO2*, ed. A. D. Code (NASA SP-310), p. 295.
Greenberg, J. M., and Chlewicki, G. 1983, *Ap. J.*, **272**, 563 (GC).
Hayes, D. S., Marko, G. E., Radick, R. R., Rex, K. H., and Greenberg, J. M. 1973, in *IAU Symposium 52, Interstellar Dust and Related Topics*, ed. J. M. Greenberg and H. C. van de Hulst (Dordrecht: Reidel), p. 83.
Jenkins, E. B., Savage, B. D., and Spitzer, L., Jr. 1986, *Ap. J.*, **301**, 355.
Johnson, H. L. 1966, *Ann. Rev. Astr. Ap.*, **4**, 193.
Jones, T. J., and Hyland, H. 1980, *M.N.R.A.S.*, **192**, 354.
Joseph, C. L. 1988, *Ap. J.*, **335**, 157.
Jura, M. 1980, *Ap. J.*, **235**, 157.
Koornneef, J. 1983, *Astr. Ap.*, **128**, 84.
Krelowski, J., Maszkowski, R., and Strobel, A. 1986, *Astr. Ap.*, **166**, 271.
Massa, D., and Savage, B. D. 1989, in *IAU Symposium 135, Interstellar Dust*, ed. L. J. Allamandola and A. G. G. M. Tielens (Dordrecht: Reidel), in press.
Mathis, J. S., and Wallenhorst, S. G. 1982, *Ap. J.*, **244**, 483.
Mathis, J. S., and Whiffen, S. G. 1989, *Ap. J.*, **341**, 805.
Rieke, G. H., and Lebofsky, M. J. 1985, *Ap. J.*, **288**, 618.
Savage, B. D., Bohlin, R. C., Drake, J. F., and Budich, W. 1977, *Ap. J.*, **216**, 291.
Savage, B. D., Massa, D., Meade, M., and Wesselius, P. R. 1985, *Ap. J. Suppl.*, **59**, 397.
Savage, B. D., and Mathis, J. S. 1979, *Ann. Rev. Astr. Ap.*, **17**, 73.
Schild, R. E. 1977, *A.J.*, **82**, 337.
Seab, C. G. 1987, in *Interstellar Processes*, ed. D. A. Hollenbach and H. J. Thronson, Jr. (Dordrecht: Reidel), p. 491.
Seaton, M. J. 1979, *M.N.R.A.S.*, **187**, 73P.
Shull, J. M., and van Steenberg, M. E. 1985, *Ap. J.*, **294**, 599.
Smith, R. G. 1987, *M.N.R.A.S.*, **227**, 943.
Snow, T. P., and York, D. G. 1975, *Ap. Space Sci.*, **34**, 19.
Underhill, A. B., and Walker, G. A. H. 1966, *M.N.R.A.S.*, **131**, 475.
Walker, G. A. H., Yang, S., Fahlman, G. G., and Witt, A. N. 1980, *Pub. A.S.P.*, **92**, 411.
Whitford, A. E. 1958, *A.J.*, **63**, 201.
Whittet, D. C. B. M. 1989, in *The Dusty Universe*, ed. M. A. Bailey and D. A. Williams (Cambridge: Cambridge University Press), in press.
York, D. G., Drake, J. F., Jenkins, E. B., Morton, D. C., Rogerson, J. B., and Spitzer, L. 1973, *Ap. J. (Letters)*, **182**, L1.

JASON A. CARDELLI, GEOFFREY C. CLAYTON, and JOHN S. MATHIS: Department of Astronomy, University of Wisconsin, 475 N. Charter Street, Madison, WI 53706